Comprehensive first-principles analysis of phonon thermal conductivity and electron-phonon coupling in different metals

Zhen Tong,[1,2] Shouhang Li,[1] Xiulin Ruan,[2] and Hua Bao[1,*]

[1]*University of Michigan-Shanghai Jiao Tong University Joint Institute, Shanghai Jiao Tong University, Shanghai 200240, China*

[2]*School of Mechanical Engineering and the Birck Nanotechnology Center, Purdue University, West Lafayette, Indiana 47907-2088, USA*

(Received 5 July 2019; revised manuscript received 17 September 2019; published 16 October 2019)

Separating electron and phonon components in thermal conductivity is imperative for understanding thermal transport in metals and highly desirable in many applications. In this work, we predict the mode-dependent electron and phonon thermal conductivities of 18 different metals at room temperature from first principles. Our first-principles predictions, in general, agree well with those available experimental data. For phonon thermal conductivity, we find that it is in the range of 2–18 W/mK, which accounts for 1%–40% of the total thermal conductivity. It is also found that the phonon thermal conductivities in transition metals and transition-intermetallic compounds (TICs) are non-negligible compared to noble metals due to the high phonon group velocities of the former. We further show that the electron-phonon coupling effect on phonon thermal conductivity in transition metals and intermetallic compounds is stronger than that of nobles, which is attributed to the larger electron-phonon coupling constant with a high electron density of states within the Fermi window and high phonon frequency in the former. For electron thermal conductivity, we observe that the transition metals and TICs have lower electron thermal conductivities compared to noble metals, which is mainly due to the weak electron-phonon coupling in noble metals. It is found that the Lorenz number of transition metals and TICs hold larger deviations from the Sommerfeld value $L_0 = 2.44 \times 10^{-8}\,\mathrm{W\,\Omega\,K^{-2}}$. We also find the mean free paths extracted at 50% accumulation function for phonons (within 10 nm) are generally smaller than those of electrons (5–25 nm).

DOI: 10.1103/PhysRevB.100.144306

I. INTRODUCTION

There have been numerous experimental measurements and theoretical analyses in order to understand the thermal transport in metals ever since the early 20th century [1–10]. It has been generally believed that free electrons make a dominant contribution to the thermal transport in metals, while the phonons make less contribution. In most applications, only the total thermal conductivity of metals is needed, so it is unnecessary to separate electron and phonon thermal conductivity. Recently, there has been growing interest in quantifying phonon heat conduction in metals, primarily driven by recent research advances in a variety of electron-phonon nonequilibrium energy transfer processes, for example, thermal transport across a metal-dielectric interface [11], laser manufacturing and laser heating [12], heat-assisted magnetic recording devices [13], etc. In addition, resolving the size effect of a metal nanostructure also requires the quantification of electron and phonon thermal conductivity and the mean free path of metals [14–17]. Therefore, how to separate the electron and phonon thermal conductivities of metals becomes an important problem, which motivates researchers to carry out various experimental and theoretical works.

In most pure metals, the electron thermal conductivity (κ_e) is believed to be much larger than the phonon thermal conductivity (κ_p). It is well known that the electrical conductivity and total thermal conductivity (κ_{total}) can be measured directly in experiments. However, it is hard to separately measure the electron and phonon thermal conductivity directly. In general, the Wiedemann-Franz law [18] is widely used to evaluate the electron thermal conductivity, in which the electron thermal conductivity is determined through the equation $\kappa_e = L\sigma T$, where κ_e is electron thermal conductivity, L is Lorenz number, and T is temperature. σ is electrical conductivity which can be experimentally determined, for example, four-probe resistivity measurement [19]. Furthermore, the phonon thermal conductivity component can then be obtained by $\kappa_p = \kappa_{\mathrm{total}} - L\sigma T$ [1,20,21]. To apply the Wiedemann-Franz law, a correct Lorenz number is needed; people usually use the Sommerfeld value [1,10] with constant $L_0 = 2.44 \times 10^{-8}\,\mathrm{V^2\,K^{-2}}$ for simplicity. However, the $L = L_0$ is only valid at the low-temperature ($T \ll \theta_D$, electron-impurity elastic scattering dominant) or high-temperature region ($T \gg \theta_D$, electron-phonon elastic scattering dominant), and L will deviate from L_0 at the intermediate-temperature region due to the inelastic electron-phonon scattering [4,22]. Because phonon thermal conductivity is a relatively small fraction, even a small error in the Lorenz number can lead to large uncertainty in the derived phonon thermal conductivity. In order to more accurately obtain phonon thermal conductivity, a few other experimental methods have been implemented, including the alloying method [5,6], superconducting method [5,23], and magnetothermal method [6,24]. However, these methods are either very complicated to conduct or limited to extremely low temperatures. Therefore, the accuracy of experimentally

*hua.bao@sjtu.edu.cn

measured κ_p is still limited and even the room-temperature values are only available for a few metals [5–9].

From the theoretical side, in order to investigate the phonon thermal conductivity of metals, the general strategy is to first estimate phonon thermal conductivity considering the phonon-phonon scattering. Some of the early efforts include the Leibfried and Schlömann [25] model, the Klemens [4] model, and the Slack [26] equation. All these analytical models only consider the phonon-phonon scattering and neglect the phonon-electron scattering. By adding the phonon-electron scattering rate, Klemens and Williams [10] proposed the formula of phonon thermal conductivity by assuming that the long-wavelength phonon modes interact with free electrons and then concluded that the phonon thermal conductivities of pure metals are in the range of 3–10 W/mK. Stojanovic *et al.* [27] developed an analytical expression of phonon thermal conductivity for metal nanostructures with the assumption of isotropic properties of the material, nearly free electron for electrons, and Debye approximation [28] for phonons. On the other hand, the expression of electron thermal conductivity at low and high temperature for monovalent metals was first derived by Wilson [29] with the assumption that only the longitudinal phonon modes interact with electrons. Makinson and Wilson [1] promoted the expressions of electron thermal conductivity for both high and low temperatures by assuming that the phonons with different polarization interact with electrons to the same extent. These theoretical treatments have significantly advanced the understanding of thermal transport in metals.

Recent advances in numerical methods have enabled more accurate prediction of phonon thermal conductivity in metals. For example, the molecular dynamic method was used to predict the phonon thermal conductivity of metals [30]. However, molecular dynamics has flaws of not only being limited by the availability and the accuracy of force fields, but also the neglect of phonon-electron coupling. In contrast, using the first-principles method, it is possible to extract the electron-phonon coupling matrix element, and then the mode-resolved electron and phonon transport properties can be obtained by combining with the Boltzmann transport equation (BTE) [31–35]. Therefore, this method can be quite useful to obtain a reliable phonon thermal conductivity of metals. The first-principles method can be ideally applied to any material. The major limitation is that very dense **k** mesh and **q** mesh used for Brillouin zone integration are needed to obtain accurate results, which requires an extremely high computational cost. In recent years, only a handful of first-principles calculations [36–39] were carried out to predict the thermal conductivity of metals. For example, Jain and McGaughey [36] predicted the electron and phonon thermal conductivity of Au, Ag, and Al including the electron-phonon scattering rate by using dense **k**-mesh (80 × 80 × 80) and **q**-mesh (32 × 32 × 32) interpolation. Wang *et al.* [37] calculated the phonon thermal conductivity of metals including aluminum (Al), noble metals (Au, Ag, Cu), and transition metals (Pt, Ni), but the accuracy of their calculated values could be limited due to the relatively coarse mesh of **k** points (16 × 16 × 16) and **q** points (16 × 16 × 16) used in the Brillouin zone integration. In our previous work [38], the intermetallic compounds NiAl and Ni_3Al were considered. These advances are important in that one can finally obtain relatively reliable values of phonon thermal conductivity in metals. However, these first-principles simulations are scattered to only a few types of metals, and the data may not be directly comparable due to the difference in their simulations, for example, the pseudopotential and Brillouin zone integration technique. Therefore, a comprehensive analysis of the phonon thermal conductivity in different types of metals is highly desirable in order to obtain more general conclusions of heat conduction in metals.

In this work, a series of first-principles calculations are carried out to predict the mode-dependent electron and phonon thermal conductivity of 18 different metals, which include noble metals, alkali-earth metals, transition metals, transition-intermetallic compounds (TICs) and noble-intermetallic compounds (NICs). The phonon thermal conductivities are calculated by considering both phonon-phonon (*p*-*p*) and phonon-electron (*p*-*e*) interactions, and the impact of phonon-electron scattering on the phonon thermal conductivity is carefully discussed. In addition, the electron thermal conductivity is evaluated by considering electron-phonon (*e*-*p*) scattering and the Lorenz numbers, as well as the mean free paths for both phonons and electrons of all 18 metals.

II. METHODS AND SIMULATION DETAILS

A. Methods

1. Phonon thermal conductivity

Combining the Boltzmann transport equation and Fourier's law [40], the phonon thermal conductivity tensor can be calculated as

$$\kappa_p^{\alpha\beta} = \sum_{\lambda} c_{v,\lambda} v_{\lambda}^{\alpha} v_{\lambda}^{\beta} \tau_{\lambda}^{p}, \tag{1}$$

where $\lambda = (\mathbf{q}, \nu)$ denotes the phonon mode with polarization ν and wave vector $\mathbf{q}$, $c_{v,\lambda}$ is the volumetric specific heat, v_{λ}^{α} and v_{λ}^{β} are the α and β component of the phonon group velocity vector v_{λ}, and τ_{λ}^{p} is the phonon relaxation time. The phonon volumetric specific heat can be obtained by using the Bose-Einstein statistics as $c_{v,\lambda} = \frac{\hbar\omega_{\lambda}}{V}\frac{\partial n_{\lambda}}{\partial T}$, where n_{λ} is the Bose-Einstein distribution function and V is the volume of the primitive cell. The group velocity can be obtained by $v_{\lambda,\alpha} = \frac{\partial\omega_{\lambda}}{\partial\mathbf{q}}$. The phonon relaxation time can be obtained using Matthiessen's [41] rule as $1/\tau_{\lambda}^{p} = 1/\tau_{\lambda}^{pp} + 1/\tau_{\lambda}^{pe}$, where $1/\tau_{\lambda}^{pp}$ denotes the *p*-*p* scattering rate which is related to the three-phonon scattering matrix element [41] and $1/\tau_{\lambda}^{pe}$ denotes the *p*-*e* scattering rate which is related to the *e*-*p* scattering matrix element [33,42].

The *p*-*p* scattering rate due to three-phonon scattering is given by Fermi's "golden rule" (FGR) [43] as

$$\begin{aligned}\frac{1}{\tau_{\lambda}^{pp}} = \frac{\pi\hbar}{16N}\sum_{\lambda_1\lambda_2}\left|V_{\lambda\lambda_1\lambda_2}\right|^2\{&(n_{\lambda_1}+n_{\lambda_2}+1)\delta(\omega_{\lambda}-\omega_{\lambda_1}-\omega_{\lambda_2})\\ &+(n_{\lambda_1}-n_{\lambda_2})[\delta(\omega_{\lambda}+\omega_{\lambda_1}-\omega_{\lambda_2})\\ &-\delta(\omega_{\lambda}-\omega_{\lambda_1}+\omega_{\lambda_2})]\},\end{aligned} \tag{2}$$

where N is the total number of phonon modes. δ is the Dirac delta function, which is approximated by a Gaussian or Lorentzian function [36] in practice. The term $V_{\lambda\lambda_1\lambda_2}$ is the

three-phonon scattering matrix element, which is related to the third-order force constants [40].

The *p-e* scattering can also be obtained from FGR [43]. Under the relaxation time approximation, the scattering rate of phonon mode λ is

$$\frac{1}{\tau_\lambda^{pe}} = \frac{2\pi}{\hbar}\sum_{\mathbf{k},i,j}\left|g^\lambda_{j\mathbf{k}+\mathbf{q},i\mathbf{k}}\right|^2(f_{i\mathbf{k}} - f_{j\mathbf{k}+\mathbf{q}})\delta(\epsilon_{i\mathbf{k}} - \epsilon_{j\mathbf{k}+\mathbf{q}} + \hbar\omega_\lambda), \tag{3}$$

where g is the *e-p* interaction matrix element, f is the Fermi-Dirac distribution function, $\mathbf{k}$ is the electron wave vector, i and j are band indices of the electron, ϵ is the energy of the electron, and ω is the phonon frequency. The *e-p* matrix element which describes an event where an electron at initial state $|i,\mathbf{k}\rangle$ is scattered to $|j,\mathbf{k}+\mathbf{q}\rangle$ by a phonon mode $\lambda = (\mathbf{q},\nu)$ is defined as [33]

$$g^\lambda_{j\mathbf{k}+\mathbf{q},i\mathbf{k}} = \sqrt{\frac{\hbar}{2\omega_\lambda}}\langle\psi_{j\mathbf{k}+\mathbf{q}}|\partial U_\lambda|\psi_{i\mathbf{k}}\rangle, \tag{4}$$

where ψ is the ground-state Bloch wave function and ∂U_λ denotes the first-order derivative of the Kohn-Sham potential with respect to the phonon displacement. In general, Eq. (3) can be further approximated because of the much smaller energy of phonons than electrons, which is expressed as [37]

$$\frac{1}{\tau_\lambda^{pe}} \approx 2\pi\sum_{\mathbf{k},i,j}\left|g^\lambda_{j\mathbf{k}+\mathbf{q},i\mathbf{k}}\right|^2\frac{\partial f(\epsilon_{i\mathbf{k}},T)}{\partial\epsilon}\delta(\epsilon_{i\mathbf{k}} - \epsilon_{j\mathbf{k}+\mathbf{q}} + \hbar\omega_\lambda)\omega_\lambda, \tag{5}$$

where $\partial f/\partial\epsilon$ is the "Fermi window" that peaks at the Fermi level.

2. Electron thermal conductivity

Combining the BTE and Onsager relations [43], the electron transport properties can be obtained as

$$\sigma_{\alpha\beta} = -\frac{e^2 n_s}{V}\sum_{i\mathbf{k}}\frac{\partial f_{i\mathbf{k}}}{\partial\epsilon}v^\alpha_{i\mathbf{k}}v^\beta_{i\mathbf{k}}\tau_{i\mathbf{k}}, \tag{6}$$

$$[\sigma S] = -\frac{en_s}{VT}\sum_{i\mathbf{k}}(\epsilon_{i\mathbf{k}} - \mu)\frac{\partial f_{i\mathbf{k}}}{\partial\epsilon}v^\alpha_{i\mathbf{k}}v^\beta_{i\mathbf{k}}\tau_{i\mathbf{k}}, \tag{7}$$

$$K_{\alpha\beta} = -\frac{n_s}{VT}\sum_{i\mathbf{k}}(\epsilon_{i\mathbf{k}} - \mu)^2\frac{\partial f_{i\mathbf{k}}}{\partial\epsilon}v^\alpha_{i\mathbf{k}}v^\beta_{i\mathbf{k}}\tau_{i\mathbf{k}}, \tag{8}$$

where $\sigma_{\alpha\beta}$ is the electrical conductivity and $S_{\alpha\beta}$ is the Seebeck coefficient of 3×3 tensors. $K_{\alpha\beta}$ is related to the electron thermal conductivity $\kappa_e = \boldsymbol{K} - \boldsymbol{S}\sigma\boldsymbol{S}T$, where T is the temperature. The summation in these three equations is over all the electrons enumerated using electronic wave vector $\mathbf{k}$ and band index i. The e is the elementary charge, n_s is the number of electrons per state, V is the volume of the primitive cell, $f_{i\mathbf{k}}$ is the Fermi-Dirac distribution, $\epsilon_{i\mathbf{k}}$ is the electron energy, μ is the chemical potential, $\mathbf{v}_{i\mathbf{k}} = \frac{1}{\hbar}\frac{\partial\epsilon_{i\mathbf{k}}}{\partial\mathbf{k}}$ is the electron velocity, α and β denote the directional components, and $\tau_{i\mathbf{k}}$ is the electron transport relaxation time. The electron transport relaxation time, limited by *e-p* scattering, can be obtained by considering the *e-p* interactions as [43]

$$\frac{1}{\tau_{i\mathbf{k}}} = \frac{2\pi}{\hbar}\sum_j\sum_\lambda\left|g^\lambda_{j\mathbf{k}+\mathbf{q},i\mathbf{k}}\right|^2\{(n_\lambda + f_{j\mathbf{k}+\mathbf{q}})\delta(\epsilon_{i\mathbf{k}} + \hbar\omega_\lambda - \epsilon_{j\mathbf{k}+\mathbf{q}}) + (n_\lambda + 1 - f_{j\mathbf{k}+\mathbf{q}})\delta(\epsilon_{i\mathbf{k}} - \hbar\omega_\lambda - \epsilon_{j\mathbf{k}+\mathbf{q}})\}. \tag{9}$$

3. Analytical models

Three-phonon scattering strength $V_{\lambda\lambda_1\lambda_2}$ in Eq. (2) is quite nontrivial. In order to obtain an expression of κ_p, Klemens [4] derived a formula of $V_{\lambda\lambda_1\lambda_2}$ by generalizing the result for long-wavelength phonons to all phonon modes, in which the Debye-like dispersion and ignorance of phonon branch restrictions were assumed. The approximation equation of $V_{\lambda\lambda_1\lambda_2}$ is as follows [4,44]:

$$\left|V_{\lambda\lambda_1\lambda_2}\right| = B\frac{M\gamma_G}{\sqrt{N}}\frac{\omega_\lambda\omega_{\lambda_1}\omega_{\lambda_2}}{v_g}\sqrt{\frac{\hbar^3}{M^3\omega_\lambda\omega_{\lambda_1}\omega_{\lambda_2}}}, \tag{10}$$

where B is a constant number, M is the total mass of atoms in the unit cell, γ_G is the average Grüneisen parameter, and v_g is the phonon group velocity in the Debye model. Although this estimation simplifies the complicated term, it is still difficult to calculate the summation in Eq. (2) due to the Dirac delta function. In order to solve this issue, Leibfried [25] used the inverse of the Debye frequency $1/\omega_D$ to approximate the Dirac delta function. With these approximations, the *p-p* scattering rate can by approximated [4,10] as $1/\tau^{pp} = B\gamma_G^2 v_g(k_B T/\mu a^3)(\omega/\omega_D)^2$, where k_B is the Boltzmann constant and μ is the shear modulus. The formula of phonon thermal conductivity which only considers *p-p* scattering can be written as follows [4,10]:

$$\kappa_p^{pp} = \frac{3.22}{B\gamma_G^2}\left(\frac{k_B\theta_D}{\hbar}\right)^3\frac{\bar{M}a}{T}, \tag{11}$$

where θ_D is Debye temperature, $\bar{M}$ is average atomic mass, a is the cube root of unit cell volume, and T is temperature. The uncertainties of this model are reflected in an uncertain numerical coefficient of B. Leibfried and Schlömann [25] give $B = 0.87$, while Klemens and Williams [10] give $B = 2$. It should be noted that there exist some debates about the value of B. Julian [45] claimed that the value given by Leibfried and Schlömann was underestimated by a factor of 0.5 due to a numerical error, which means Julian gave a corrected value of $B = 1.74$. Furthermore, Julian [45] also tried to fit the coefficient of B using Grüneisen parameters. By using Julian's fitting parameters, Slack [26] presented the expression for the phonon thermal conductivity (only *p-p* scattering) as follows:

$$\kappa_p^{pp} = \frac{0.849\times3\sqrt[3]{4}}{20\pi^3\left(1 - 0.514\gamma_G^{-1} + 0.228\gamma_G^{-2}\right)}\left(\frac{k_B\theta_D}{\hbar}\right)^2\frac{k_B\bar{M}a}{\hbar\gamma_G^2}. \tag{12}$$

In general, only considering *p-p* scattering to determine the phonon thermal conductivity in metals is not accurate due to the importance of phonon-electron scatterings. However, the phonon-electron scattering strength is very complicated as shown in Eq. (3). In order to obtain the expression for the phonon-electron scattering rate corresponding

to a phonon relaxation process, the electrons are treated as free electrons of Fermi energy E_f and Fermi velocity v_0 to interact with phonons and then the phonon-electron scattering rate can be written as the form [4,10] $1/\tau^{pe} = \pi/3(v_g/v_0)(n_e C_{pe}^2 \omega/\mu a^3 E_f)$, where n_e is the number of electrons per atom. C_{pe} is the phonon-electron interaction parameter which has a magnitude comparable to E_f [10,22]. Although the terms have been simplified, the values of them in the approximated equations are still difficult to determine, such as C_{pe}. With the help of these approximated relaxation time terms, Klemens and Williams [10] gave the phonon thermal conductivity considering both *p*-*p* and *p*-*e* scattering schemes as follows:

$$\kappa_p^{pp+pe} = \kappa_p^{pp}\left[1 - \frac{\omega_i}{\omega_D}\ln\left(\frac{\omega_D}{\omega_i} + 1\right)\right], \tag{13}$$

where $\omega_i = \omega_D(v_g/v_0)(n_e\pi/3B\gamma_G^2)(C_{pe}^2/k_B T E_f)$. With further simplification, we find that ω_i/ω_D equals τ^{pp}/τ^{pe} with the above approximated relaxation time terms of τ^{pp} and τ^{pe}. It should be noted that the phonon thermal conductivity calculated by using these analytical formulas will be compared with the first-principles calculations, which will help us understand the accuracy of these approximated models.

B. First-principles calculations

The first-principles calculations including density functional theory (DFT) and density functional perturbation theory (DFPT) are carried out using the QUANTUM ESPRESSO package [46] to predict the phonon and electron thermal transport in these metals by considering *p*-*p* and *p*-*e* scatterings. In *p*-*p* scattering rate calculations, the second-order interatomic force constants (2nd IFCs) are obtained using DFPT and the 3rd IFCs are obtained using the finite-difference supercell methods in which the forces are extracted from the self-consistent field calculation of displaced supercell configurations. In order to calculate the 3rd IFCs, the supercell is created by using the THIRDORDER.PY package [47]. The size of supercell and nearest neighboring (NN) atoms are provided in Sec. S2 of the Supplemental Material (SM) [48]. The phonon thermal conductivity by considering different NN atom cutoffs in 3rd IFCs is studied and the convergence calculation is shown in Sec. S4.1 of the SM [48]. In the *p*-*e* scattering rate calculations, the phonon perturbation is first calculated using DFPT as implemented in QUANTUM ESPRESSO [46] and then the *e*-*p* scattering matrix element is calculated in ELECTRON-PHONON WANNIER (EPW) package [49]. The *e*-*p* scattering matrix element is initially obtained on coarse electron and phonon wave-vector grids and then interpolated to denser electron and phonon wave-vector grids using the maximally localized Wannier functions [50] basis as implemented in EPW [49]. The energy window used in the electron-phonon matrix calculations is set as 1.5 eV. The denser meshes of wave vector for calculating the *e*-*p* scattering rate are listed in Sec. S3 of the SM [48]. In these calculations, the norm-conserving pseudopotentials [51] are used. The exchange and correlation (XC) functional is treated by local density approximation (LDA) [52] or generalized gradient approximation (GGA) [53] in our calculations. The choice of XC functional depends on the material, and it is determined by searching the literature with suggested XC functional for the corresponding material.

It should be noted that the following factors may have effects on the predicted values of thermal conductivity and electrical conductivity from first-principles calculations: (1) pseudopotentials used in DFT calculations [37], (2) the number of **k** and **q** meshes used in the interpolation process during electron-phonon scattering rate calculations [36], and (3) the method such as the relaxation time approximation (RTA) or iterative scheme used for calculating the thermal conductivity [54]. Here, we choose the pseudopotentials that ensure the DFT calculated electrical conductivity matches well with the experimental values. We also investigated the effect of **k** and **q** meshes on the electrical conductivity and electron thermal conductivity as shown in Secs. S4.2 and S4.3 in the SM [48], and then the **k** and **q** meshes were finally determined as presented in Table S2 of Sec. S3 in the SM [48] based on the balance of accuracy and computational cost. In addition, we use the RTA method which can guarantee the denser **q** mesh used in three-phonon scattering rate calculations. Actually, it has been reported that the difference of the calculated electrical conductivity between the momentum-RTA and the iterative method is almost negligible for Al [54], and Ma *et al.* [55] found the momentum-RTA method can match the iterative method well at intermediate and high temperatures. Besides, such method was also widely used to predict the electronic thermal conductivity of other metals [27,36]. Therefore, it should be proper to employ the RTA method to predict the electron thermal conductivity in the present work.

III. RESULTS AND DISCUSSION

A. Electrical conductivity, and electron and phonon thermal conductivity

By implementing the first-principles calculations, the electrical conductivity σ, and phonon κ_p and electron κ_e thermal conductivity are obtained as shown in Table I. It should be mentioned that the spin-orbital coupling (SOC) effect has been considered in the heavy metals such as Ni, Pt, Pd, Co, Ti, Mn, CoAl, and TiAl, in which the Pt is also used as an example to analyze the SOC and noSOC effect on the electrical conductivity as shown in Sec. S5 of the SM [48]. First, we can see that the predicted σ, in general, agree well with experimental data [10,22,56–60]. The difference is in the range of 2%–31%, with most within 15%, which is acceptable. We can also see that the DFT predicted $\kappa_{\text{total}}^{\text{DFT}} = \kappa_e + \kappa_p$ at room temperature agree well with experimental values $\kappa_{\text{total}}^{\text{Expt.}}$ [10,22,56–60] as presented in Table I. To further validate our calculations, the DFT optimized lattice constants and phonon dispersion curves are compared with the experimental values, and the DFT predicted band structures are compared with the Wannier interpolated band structures. We find that they are in good agreement, as shown in Table S1 and Sec. S7 of the SM [48]. All of these comparisons and validations provide confidence for us to further analyze *e*-*p* coupling strength and its effect on phonon thermal conductivity.

From Table I, we note that the phonon thermal conductivity ranges from 2 to 18 W/mK. The ratio of phonon thermal conductivity to total thermal conductivity $\kappa_p/\kappa_{\text{total}}$ can be

TABLE I. The DFT predictions of electrical conductivity σ and total thermal conductivity $\kappa_{\text{total}}^{\text{DFT}} = \kappa_e + \kappa_p$ are compared to experimental values at room temperature [10,22,56–60]. κ_e denotes for electron thermal conductivity, κ_p for phonon thermal conductivity, and $\kappa_{\text{total}}^{\text{Expt.}}$ for experimental value. $L_0 = \pi^2 k_B^2/(3e^2) = 2.44 \times 10^{-8}\ \text{V}^2\ \text{K}^{-2}$ is the Sommerfeld value of the Lorenz number [10], $L = \kappa_e/(\sigma T)$, where T is temperature.

	σ ($\times 10^7\ \Omega^{-1}\ \text{m}^{-1}$)		κ_p (W/mK)	κ_e (W/mK)	$\kappa_{\text{total}}^{\text{DFT}}$ (W/mK)	$\kappa_{\text{total}}^{\text{Expt.}}$ (W/mK)	$\kappa_p/\kappa_{\text{total}}^{\text{DFT}}$ (%)	$\frac{L}{L_0}$
Material	DFT	Expt.	DFT	DFT	DFT	Expt.	DFT	DFT
Ag	6.26	6.21	5.69	450.86	456.55	436.00	1.25	0.98
Au	3.63	4.50	2.80	273.45	276.25	318.00	1.01	1.03
Cu	5.27	5.78	17.42	361.32	378.74	402.00	4.60	0.94
Al	3.37	4.12	8.95	232.53	241.49	237.00	3.71	0.94
Mg	2.43	2.30	7.15	178.20	185.35	153.00	3.86	1.00
Pt	1.23	1.02	6.49	89.75	96.24	71.90	6.74	1.00
Pd	0.82	1.03	12.51	76.60	89.11	71.70	14.04	1.28
Ni	1.51	1.60	15.33	84.53	99.86	93.00	15.35	0.76
Ti	0.38	0.25	5.32	25.31	30.63	22.30	17.37	0.91
Co	1.16	1.67	12.99	78.65	91.65	99.00	14.18	0.92
Mn	0.08	0.07	3.02	4.98	8.00	7.80	37.74	0.86
NiAl	0.86	1.02	6.02	63.89	69.91	76.00	8.61	1.02
Ni_3Al	0.43	0.30	4.72	31.95	36.66	28.50	12.86	1.02
TiAl	0.10	0.13	5.17	7.34	12.51	11.50	41.32	0.96
FeAl	0.13	0.18	3.24	8.49	11.72	12.00	27.61	0.90
CoAl	0.59	0.71	4.83	40.85	45.67	37.00	10.57	0.95
Cu_3Au	1.66	1.85	1.89	118.36	120.25	157.20	1.57	0.98
CuAu	1.83	2.50	2.32	132.46	134.78	167.00	1.72	0.99

smaller than 2% or as large as 40% at 300 K. Eight out of 18 metals have phonon contributions of more than 10%, which is non-negligible. Furthermore, κ_p can play a more important role in the thermal conductivity of metallic nanostructure due to the significant reduction of κ_e at the nanostructure [27]. Therefore, our calculation results show the necessity of first-principles investigation on the phonon thermal transport in metals.

In addition, the predicted κ_p including both *p-p* and *p-e* scattering from first principles are compared with the predictions by the Klemens model [10] [Eq. (13)], and the comparisons are shown in Fig. 1. It should be noted that the average relaxation times of τ^{pp} and τ^{pe} calculated from first principles were used in Eq. (13). We can see that the Pearson correlation between the first-principles prediction and the theoretical Klemens prediction is 0.25. It indicates that the Klemens model fails to accurately predict the phonon thermal conductivity. This is not surprising since the Klemens model was derived based on the assumption of Debye approximation, free electrons interacting with phonons, and the long-wavelength phonons [10]. Therefore, the previous phonon thermal conductivity estimations of metals from the Klemens model have large uncertainty and must be used with care.

B. Phonon thermal conductivity with only *p-p* scattering

The above calculations provide relatively reliable data for the phonon thermal conductivity of different types of metals. To gain deeper insights into the phonon thermal conductivity of metals, further analysis is necessary. As shown in Eqs. (2) and (3), the phonon thermal conductivity in metals is affected by both *p-p* and *p-e* scattering. Therefore, we first investigate the phonon thermal conductivity only considering *p-p* scattering, and then further consider electron-phonon coupling effect on the phonon thermal conductivity.

The first-principles calculated phonon thermal conductivities κ_p^{pp} (only *p-p* scattering is considered) at 300 K are shown

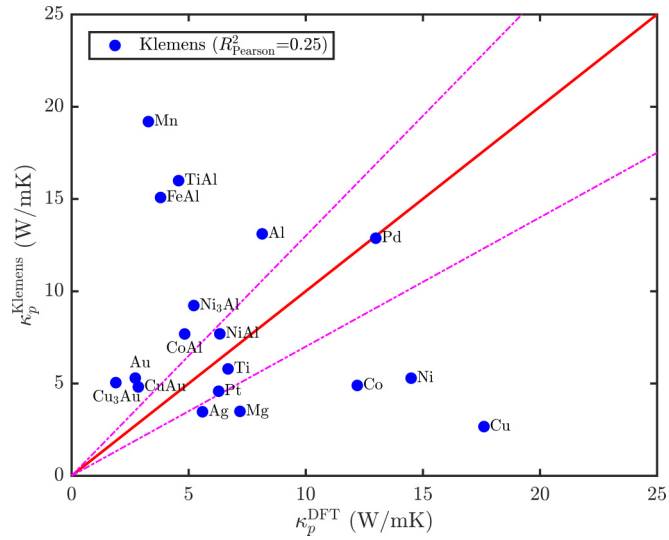

FIG. 1. Phonon thermal conductivity κ_p predictions at a temperature of 300 K from first-principles calculations and the Klemens model [10], which include both *p-p* and *p-e* scattering. The dashed line represents ±30% error.

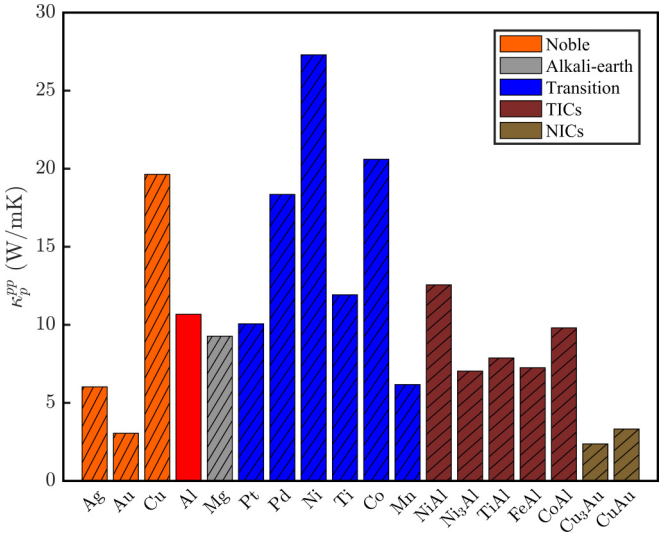

FIG. 2. Phonon thermal conductivity κ_p^{pp} of noble, alkali earth, transition, TICs, and NICs at 300 K. Here, only p-p scattering is considered in the calculation of phonon thermal conductivity.

in Fig. 2. The values of κ_p^{pp} are within the range of 2–30 W/mK. While most of the metals have κ_p^{pp} smaller than or approaching 10 W/mK, there are a few exceptions, including Cu, Pd, Ni, and Co. These are all elemental metals with relatively small atomic masses. Except for Cu which is a noble metal, all others are transition metals. In order to make further analysis of the phonon thermal conductivity, one can see that the phonon thermal conductivity from Eq. (1) is related to both group velocity and relaxation time. Therefore, we plot the mode-dependent p-p scattering rate $1/\tau_\lambda^{pp}$ and phonon group velocity v_λ^{ph} for a few representative materials for comparison, including Ag (noble), Mg (alkali earth), Ni (transition), TiAl (TICs), and CuAu (NICs), as shown in Fig. 3. We can see that the p-p scattering rates for these metals are comparable in Fig. 3(a). However, the phonon group velocity of transition metal (Ni) is larger than that of noble metal (Ag) and it is also larger for TICs (TiAl) compared to NICs (CuAu) as shown in Fig. 3(b). From the comparison, we can see that the phonon group velocity is the dominant factor in causing the differences in phonon thermal conductivity. On the other hand, it is well known that the materials with smaller atomic mass and stronger bonding generally have higher phonon group velocity. Therefore, it is not surprising that these materials (like Pd, Pt, Ti, Ni, Co, Mn) have relatively higher κ_p^{pp} than that of noble metals (like Ag, Au), since transition metals generally have stronger bonding [61] as compared to other metals. This statement is supported by the binding energy of these materials as shown in Table II. In addition, by comparing the phonon group velocity and p-p scattering rate of the metals with that of a good semiconductor of silicon (∼150 W/mK) as shown in Fig. 3, we find that the metals have much larger p-p scattering rate and lower phonon group velocity than silicon. In fact, this is because covalent bonding in silicon is usually stronger than the metallic bonding in metals [61].

Furthermore, in the analytical models, the strength of p-p scattering and phonon group velocity are usually quantified by the Grüneisen parameter γ_G and Debye temperature θ_D,

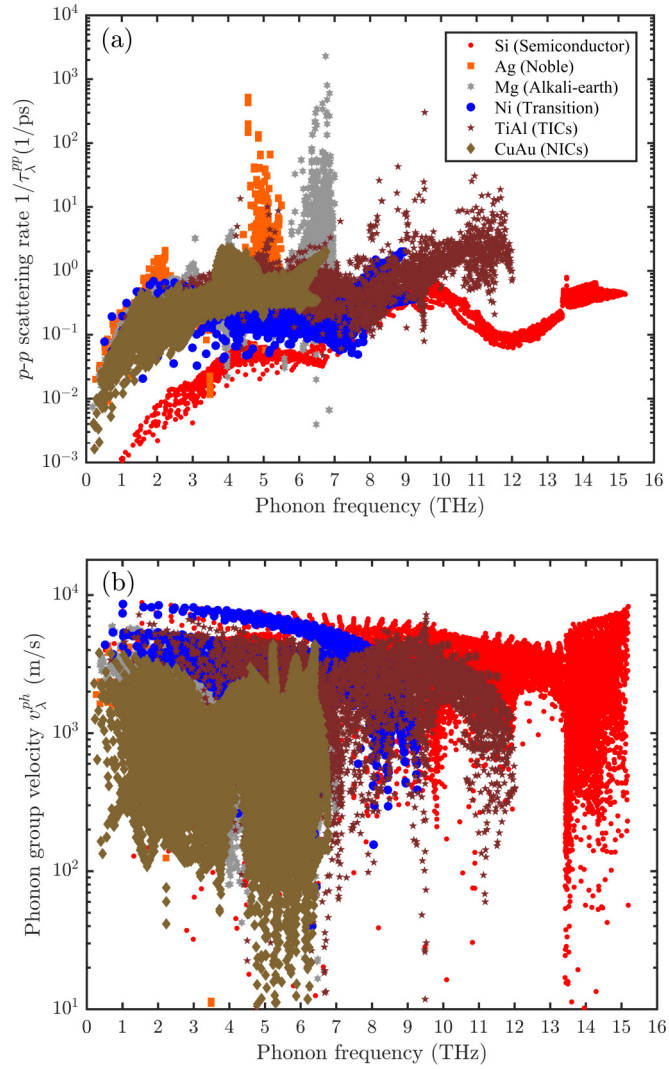

FIG. 3. (a) Phonon-phonon scattering rate and (b) phonon group velocity for Ag (noble), Mg (alkali earth), Ni (transition), TiAl (TICs), CuAu (NICs), and Si (semiconductor) at 300 K.

respectively. Here, we also present the predicted values of γ_G and θ_D, as shown in Table II, and the values agree well with experimental values (see SM, Sec. S6 [48]). The variation of κ_p^{pp} with γ_G and θ_D are also plotted as shown in Fig. 4. Overall, we can see that κ_p^{pp} is larger with higher θ_D and smaller γ_G. This is also consistent with the general theory for phonon thermal conduction, which says that the larger phonon group velocity (strong bonding with high θ_D) and smaller p-p scattering rate (weak anharmonicity with small γ_G) result in larger phonon thermal conductivity. The Pearson correlation coefficients between κ_p^{pp} and the parameters are 0.26 and 0.12 for θ_D and γ_G, respectively, indicating that the group velocity is more important in determining the phonon thermal conductivity, but neither of the two parameters can be directly used to evaluate κ_p^{pp}.

Since classical thermal conductivity models were widely used to estimate the phonon thermal conductivity of metals [4,62], we can also check their accuracy. The predicted κ_p^{pp} from first principles are compared with the predictions by the

TABLE II. DFT predicted values of Debye temperature θ_D, Grüneisen parameter γ_G, κ_p^{pp} (only *p-p* scattering is considered), κ_p^{pp+pe} (both *p-p* and *p-e* scattering are considered), and reference data [27,36,37] for κ_p^{pp+pe}. DFT predicted *e-p* coupling constant λ_{ep} and experimental values [12,64–66] of λ_{ep}. DFT predicted binding energy of some elemental metals.

	Debye (K)	Grüneisen parameter	Binding energy (eV)	Phonon thermal conductivity at 300 K (W/mK)			*e-p* Coupling constant	
Material	θ_D (DFT)	γ_G (DFT)	(DFT)	κ_p^{pp} (DFT)	κ_p^{pp+pe} (DFT)	κ_p^{pp+pe} (Literature)	λ_{ep} (DFT)	λ_{ep} (Expt.)[a]
Ag	228.18	2.69	2.61	6.03	5.69	9.3,[b] 5.2,[c] 4.0[d]	0.13	0.13
Au	184.17	3.00	3.38	3.05	2.80	5.0,[b] 2.6,[c] 2.0[d]	0.18	0.15
Cu	335.4	1.94	4.85	19.49	17.42	22.2,[b] 16.9[c]	0.14	0.14
Al	397.26	2.45	3.53	10.02	8.95	21.1,[b] 5.8,[c] 6.0[d]	0.43	0.43
Mg	343.35	1.71	4.82	9.27	7.15		0.25	0.27
Pt	243.48	1.58	5.70	8.67	6.49	8.3,[b] 5.8[c]	0.58	0.66
Pd	275.13	1.62	5.18	19.62	12.51		0.45	0.41
Ni	437.16	1.53	5.21	27.79	15.33	42.2,[b] 23.2[c]	0.36	0.31
Ti	380.54	1.12	5.18	11.92	5.32		0.30	0.38
Co	353.83	1.53	5.99	20.60	12.99		0.56	
Mn	352.09	1.17	8.14	6.17	3.02		0.46	
NiAl	349.45	1.86		12.31	6.02		0.29	
Ni_3Al	321.72	1.88		7.78	4.72		0.30	
TiAl	337.24	1.23		7.88	5.17		0.57	
FeAl	338.01	1.32		7.25	3.24		0.50	
CoAl	379.66	1.46		9.81	4.83		0.46	
Cu_3Au	251.71	2.04		2.37	1.89		0.34	
CuAu	228.17	2.03		3.32	2.32		0.31	

[a]References [12,64–66].
[b]Reference [27].
[c]Reference [37].
[d]Reference [36].

widely used Klemens model [4] [Eq. (11)] and Slack model [26] [Eq. (12)], as shown in Fig. 5. It should be noted that the first-principles calculated Debye temperature and Grüneisen parameter are used in both the Klemens and Slack models. We can see that the Pearson correlation between first-principles prediction and theoretical prediction is only 0.56 and 0.52 for the Klemens and Slack models, respectively, indicating that these analytical models fail to accurately predict the phonon thermal conductivity. This is not surprising since these analytical models generally adopt the Debye approximation and the long-wavelength assumption is employed in the Klemens model [10]. Comparing to semiconductors and dielectrics [44], these models are not reliable for metals, presumably because they were originally developed for nonmetallic materials [25]. As such, the previous phonon thermal conductivity estimations from these models [10,27,63] have large uncertainty and must be used with care.

C. Electron-phonon coupling effect on phonon thermal conductivity

The *p-e* scattering is an important scattering term in the phonon scattering process for metals and it should be rigorously considered. It was believed that the *p-e* scattering term makes a relatively small contribution to phonon thermal conductivity at medium-temperature range [10,22,36,37]. However, such statement cannot be completely supported by our results. Here, we quantified the reduction $(\kappa_p^{pp} - \kappa_p^{pp+pe})/\kappa_p^{pp}$ of κ_p^{pp} after including the *p-e* scattering effect as shown in Fig. 6 and the data values are also presented in Table II. The *e-p* coupling effect on phonon thermal conductivity κ_p^{pp} appears to vary strongly with different metals.

To understand how the scattering with electrons affects the phonon thermal conductivity, we first examine the expression of *p-e* scattering rate $1/\tau_\lambda^{pe}$ in Eq. (5) to figure out the determining factors on the strength of *p-e* scattering rate. With the summation of the product of $|g^{\lambda}_{j\mathbf{k}+\mathbf{q},i\mathbf{k}}|^2$ and $\frac{\partial f(\epsilon_{i\mathbf{k}},T)}{\partial \epsilon}\delta(\epsilon_{i\mathbf{k}} - \epsilon_{j\mathbf{k}+\mathbf{q}} + \hbar\omega_\lambda)\omega_\lambda$ in Eq. (5), we can see that the strong *p-e* scattering rate generally comes from three conditions: (I) high electron density of states around the Fermi surface, (II) high phonon frequency, (III) large *e-p* coupling matrix element. The high electron density of states within the Fermi window provides more available electron state for *e-p* scattering, which results in a stronger *e-p* interaction. The strong *e-p* interaction is manifested by a high *e-p* coupling constant λ_{ep} [31,33] which describes all the possible combinations with $\epsilon_{i\mathbf{k}}$ and $\epsilon_{j\mathbf{k}+\mathbf{q}}$ on the Fermi surface under the perturbation of phonon with frequency ω_λ. In other words, the satisfaction of conditions I and III makes high λ_{ep}, but it does not always ensure large *p-e* scattering rate. If the material has high phonon frequencies which equal the energy difference between $\epsilon_{j\mathbf{k}+\mathbf{q}}$ and $\epsilon_{i\mathbf{k}}$ states, the $\delta(\epsilon_{i\mathbf{k}} - \epsilon_{j\mathbf{k}+\mathbf{q}} + \hbar\omega_\lambda)\omega_\lambda$ will be larger.

Based on these theoretical understandings and combining the data in Fig. 6 and Table II, we can draw the following conclusions. First, transition metals (Pt, Pd, Ni, Ti, Co, Mn) have a stronger *e-p* coupling effect than that of noble metals

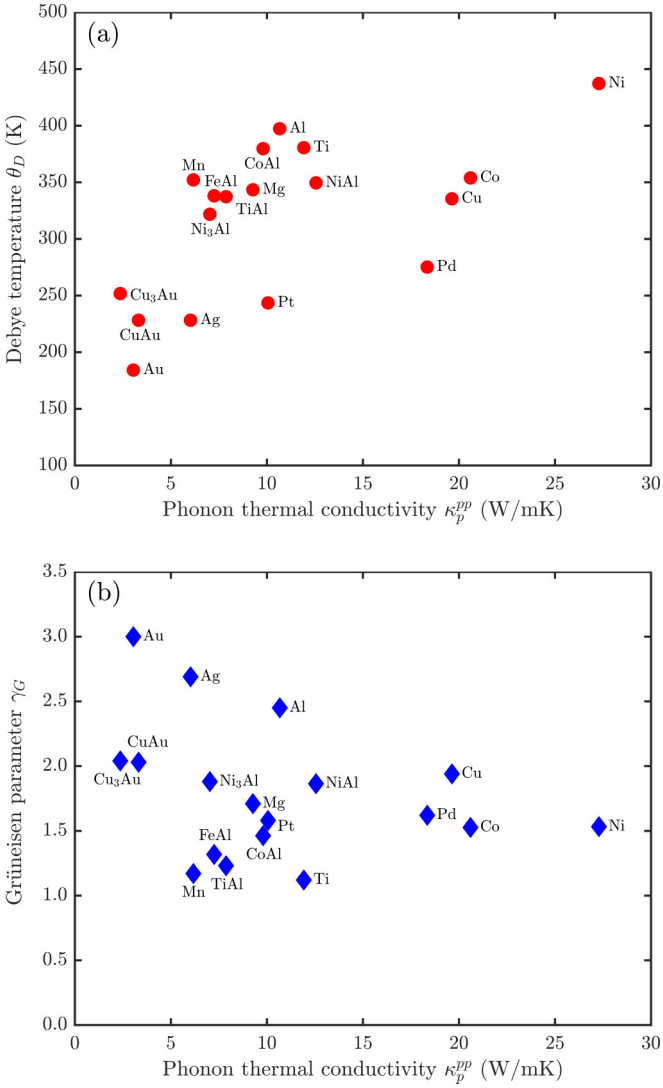

FIG. 4. The phonon thermal conductivity κ_p^{pp} variation with (a) Debye temperature θ_D and (b) Grüneisen parameter γ_G at 300 K.

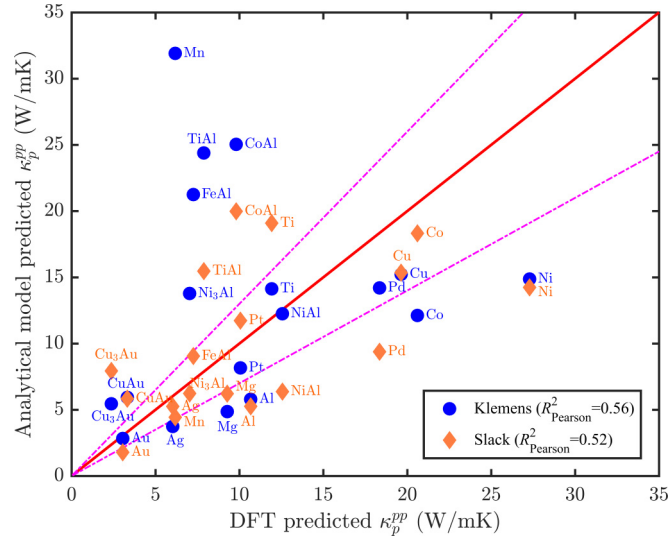

FIG. 5. Phonon thermal conductivity predictions at a temperature of 300 K from first-principles calculations and theoretical calculations using the Klemens [10] and Slack models [26], which only consider the *p-p* scattering. The dashed line represents ±30% error.

(Au, Ag, Cu), due to their higher electron density of states near the Fermi surface (see the electron density of states in the SM, Sec. S7 [48]), larger *e-p* coupling constant λ_{ep}, and higher phonon frequency (see the phonon dispersion curve in Sec. S7 of the SM [48]). Second, if the material satisfies only one of the conditions (high λ_{ep} or high ω_λ), the *e-p* coupling effect is generally weaker than that of materials with both high λ_{ep} and high ω_λ. For example, the TICs (FeAl, CoAl, NiAl, Ni_3Al, TiAl) have both larger λ_{ep} (>0.2) and higher phonon frequency ω_λ compared to NICs (CuAu, Cu_3Au) with only higher λ_{ep} but lower ω_λ. In other words, TIC atoms are lighter than NICs and will cause higher phonon frequency as well as be easier to satisfy condition II under the condition of comparable λ_{ep}. This can be further demonstrated by the mode-dependent electron-phonon coupling matrix $|g|$ as shown in Fig. 7, in which the $|g|$ of NiAl (TICs) and CuAu (NICs) are plotted for comparison. It can be seen that the $|g|$ of NiAl is higher than that of CuAu with comparable λ_{ep} ($\lambda_{ep}^{\mathrm{NiAl}} = 0.29$ and $\lambda_{ep}^{\mathrm{CuAu}} = 0.31$), which indicates that the higher phonon frequency of NiAl induces stronger *e-p* coupling than CuAu as shown in Fig. 7. Therefore, TICs have a stronger *e-p* coupling effect.

Third, the CuAu and Cu_3Au have a stronger *e-p* coupling effect than that of Cu and Au, which is due to the participation of optical phonons in the electron-phonon interactions within CuAu and Cu_3Au but no optical phonons in Cu and Au. This can be explained through the Eliashberg spectral function $\alpha^2F(\omega)$ which is generally used to quantify the phonon frequency contribution to the *e-p* coupling strength [31]. The $\alpha^2F(\omega)$ of CuAu and Cu_3Au is plotted as shown in Fig. 8; we can see that the optical phonon contribution to $\alpha^2F(\omega)$ is considerable. This result tells us that the optical phonon in CuAu and Cu_3Au makes a great contribution to the *e-p* coupling. In addition, the electron density of states of Al and

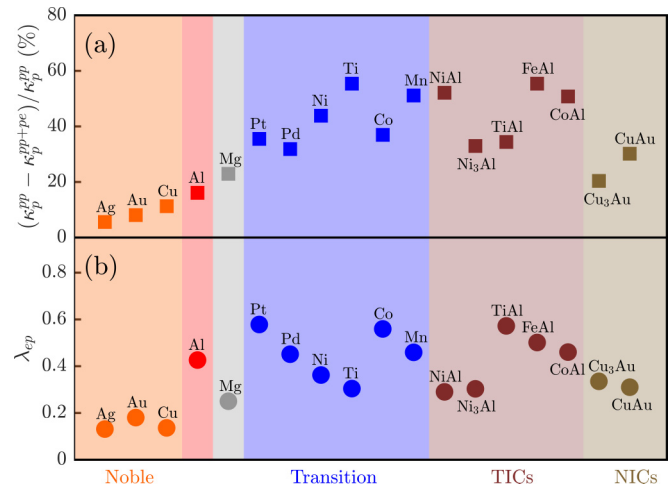

FIG. 6. (a) Percentage of the reduction of phonon thermal conductivity κ_p^{pp} induced by electron-phonon coupling effect. (b) Electron-phonon coupling constant λ_{ep}.

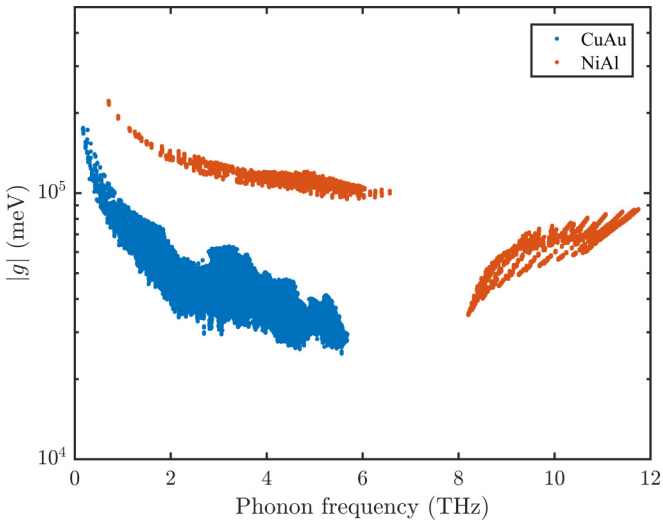

FIG. 7. Electron-phonon coupling matrix of NiAl and CuAu.

the alkali-earth metal (Mg) behave like the density of states of a free electron, which induces high electron density of states within the Fermi window (see SM, Sec. S7 [48]). Therefore, the *e-p* coupling effects in Al and Mg are stronger compared to noble metals which have low electron density of states within the Fermi window although they have comparable ω_λ (see SM, Sec. S7 [48]).

D. Electron and phonon contribution to thermal conductivity

By using the first-principles predicted κ_e and σ, we calculated the L at 300 K and compared it with the L_0 as shown in Table I. It can be seen that the deviation between L and L_0 varies between 1% and 17%, which indicates that the

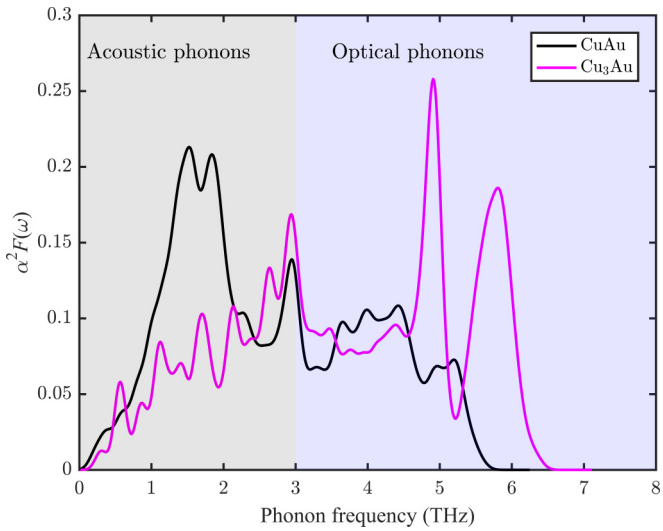

FIG. 8. Variation of Eliashberg spectral function $\alpha^2F(\omega)$ with phonon frequency for CuAu and Cu_3Au. The gray region represents the phonon frequency for acoustic phonons and the blue region for optical phonons. It should be stated that the separating point of the acoustic and optical phonon is at about 3 THz for both CuAu and Cu_3Au, which is shown in the SM, Sec. S7 [48].

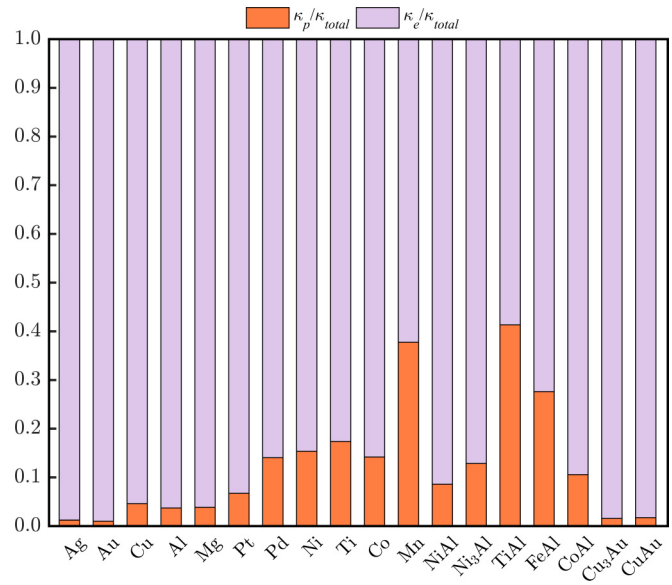

FIG. 9. The percentage of phonon and electron thermal conductivity contributing to total thermal conductivity for these 18 metals.

general treatment of evaluating electron thermal conductivity by using L_0 should be done carefully even for certain metals. In addition, we also analyzed phonon and electron contribution to the total thermal conduction as shown in Fig. 9. We can see that the phonon contribution can be neglected with $\kappa_p/\kappa_{\text{total}}$ less than 10% for noble metals, alkali earths and NICs, but it could be non-negligible for transition and TICs with $\kappa_p/\kappa_{\text{total}}$ ranging between 10% and 40% though their absolute values of κ_p range from 3 to 15 W/mK. Actually, for noble metals, the *e-p* scattering is very weak compared to transition metals, which makes their electrical conductivity much larger than that of transition metals as seen in Table I. Therefore, the electron thermal conductivity is high for noble metals, leading to a relatively much smaller phonon component of thermal conductivity. On the other hand, the phonon component of thermal conductivity in the transition metals and intermetallic compounds is comparable as discussed in Sec. III C. Combing these two factors in transition metals and intermetallic compounds, it is not surprising that the total thermal conductivity of them is low as seen in Table I and the phonon component of thermal conductivity is large as seen in Fig. 9 compared to the noble metals.

E. Electron and phonon mean free path

With the development of nanoelectronic devices [13–17], metal structures with nanoscale dimension were widely used. However, the thermal conductivities of nanostructures are significantly different from their bulk values, and the size effect generally induces reductions due to the scattering of electrons and phonons at surfaces and by grain boundaries. In order to figure out the size effect on the thermal conductivity, the mean free path (MFP) for both phonons and electrons was calculated. The MFP denoted by Λ is a measure of the distance traveled by a carrier between scattering events and is

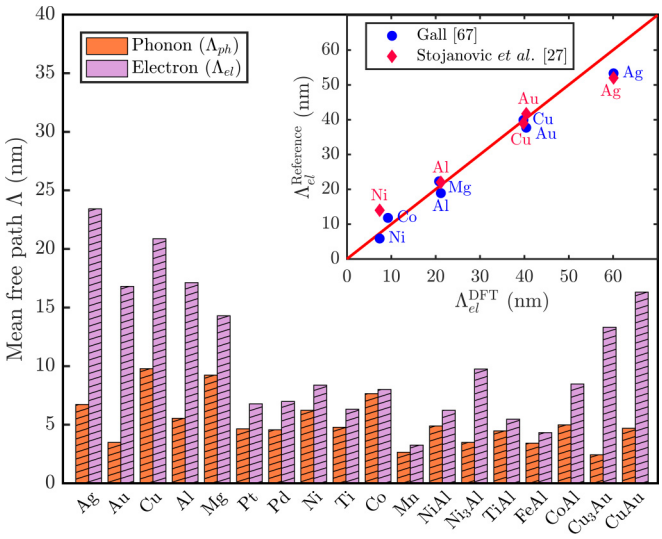

FIG. 10. Average phonon and electron mean free path of 18 metals at 300 K. The inset plot is the comparison of electron MFP between our calculated values and reference data [27,67].

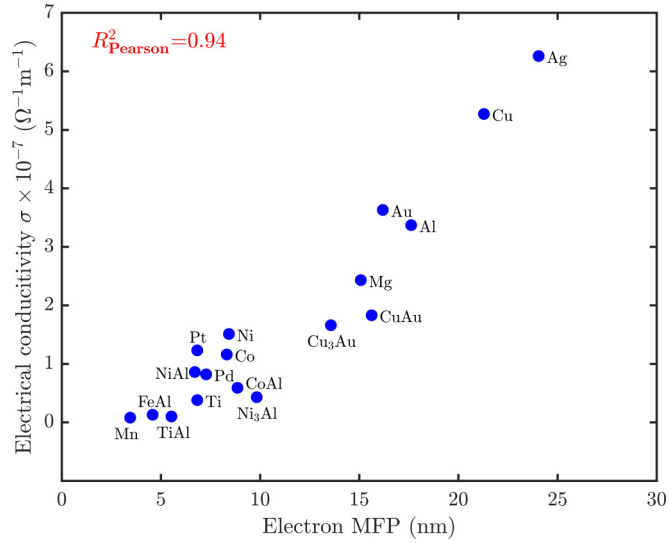

FIG. 11. Variation of electrical conductivity with electron MFPs for 18 metals at 300 K.

the product of the magnitude of its velocity and lifetime (e.g., for phonon mode λ, $\Lambda_\lambda = |v_\lambda|\tau_\lambda$).

The average mean free path can have different definitions. Also, the mean free path for electric conduction and electron thermal conductivity can be different. Here, since we focus on thermal conductivity, the average electron and phonon MFP is defined through the accumulation function (see SM, Sec. S9 [48]) which describes the contributions of carriers with different MFPs to thermal conductivity. The final values of Λ are extracted at 50% of the thermal conductivity accumulation function and the results are shown in Fig. 10. We also compare our calculated electron MFPs with the available reference data [27,67] as shown in the inset of Fig. 10. It should be noted that the MFP in the inset plot is calculated with the definition of Gall's [67] work to make a fair comparison. We can see that our calculated values agree well with the reference data. Importantly, it can be found that the phonon MFP is within 10 nm for all the 18 metals while the electron MFP ranges from 5 to 25 nm. The electron MFPs of nobles are larger than transition metals as expected. In addition, we can see that the MFPs of electrons are in general larger than that of phonons, which indicates the electron thermal conductivity will show a stronger size effect than the phonon thermal conductivity in metal nanostructures. Furthermore, in order to understand the function of electron MFP in determining the electron transport properties, we plot the variation of electrical conductivity with electron MFPs extracted at 50% of electrical conductivity as shown in Fig. 11. We can see that the materials with large electron MFPs generally have high electrical conductivity and the Pearson correlation between them is 0.94, which indicates that the transport properties of electrons are strongly correlated to the electron MFPs. By using these data, we further give a linear fitting relation with a slope of 0.4737 (correlation with $R^2 = 0.43$) between electron MFP (nm) and electrical conductivity ($\Omega^{-1}\,\mu m^{-1}$) to predict the electron MFP if the electrical conductivity is known.

IV. SUMMARY

In summary, first-principles calculations are conducted to predict the mode-dependent thermal properties of 18 metals including noble metals, transition metals, alkali-earth metals, noble-intermetallic compounds, and transition-intermetallic compounds at room temperature. The first-principles predicted values of thermal conductivity and electrical conductivity agree well with experimental results. The first-principles data allow the quantification and the separation of the electron and phonon contributions to thermal conductivity. We find that phonon thermal conductivities which only consider phonon-phonon scattering are within a range of 2–30 W/mK, in which the phonon group velocity is the dominant factor of determining the phonon thermal conductivity. The phonon thermal conductivities become 2–18 W/mK when the phonon-electron scattering is included, and account for 1%–40% in the total thermal conductivity. Moreover, we find that the electron-phonon coupling effect on phonon thermal conductivity in transition metals and intermetallic compounds is stronger than that of nobles, which is mainly due to the large electron-phonon coupling constant with a high electron density of states within the Fermi window and high phonon frequency. In addition, noble metals have high electron thermal conductivity in the range of 265–476 W/mK mainly due to weak electron-phonon coupling. Besides, the calculated Lorenz numbers for all 18 metals show considerable deviations from the Sommerfeld value $L_0 = 2.44 \times 10^{-8}\,V^2\,K^{-2}$ in transition metals and TICs. Finally, it is shown that the MFPs at 50% accumulation function for phonon (within 10 nm) are generally smaller than those of electron (5–25 nm), which yields important insights on size effect in metal nanostructures.

ACKNOWLEDGMENTS

Z.T., S.L., and H.B. acknowledge the support by the National Natural Science Foundation of China (Grant No.

51676121) and the Materials Genome Initiative Center of Shanghai Jiao Tong University. Simulations were performed at the Center for High Performance Computing (π) of Shanghai Jiao Tong University. Z.T. also acknowledges the financial support of the Chinese Scholarship Council (CSC, Grant No. 201806230169).

[1] R. E. B. Makinson and A. H. Wilson, Math. Proc. Cambridge Philos. Soc. **34**, 474 (1938).
[2] C. C. Bidwell, Phys. Rev. **58**, 561 (1940).
[3] P. G. Klemens, Aust. J. Phys. **7**, 57 (1953).
[4] P. G. Klemens, in *Solid State Physics*, edited by F. Seitz and D. Turnbull (Academic Press, New York, 1958), pp. 1–98.
[5] H. N. D. Lang, H. van Kempen, and P. Wyder, J. Phys. F: Met. Phys. **8**, L39 (1978).
[6] W. H. Butler and R. K. Williams, Phys. Rev. B **18**, 6483 (1978).
[7] R. K. Williams, D. W. Yarbrough, J. W. Masey, T. K. Holder, and R. S. Graves, J. Appl. Phys. **52**, 5167 (1981).
[8] R. K. Williams, R. S. Graves, T. L. Hebble, D. L. McElroy, and J. P. Moore, Phys. Rev. B **26**, 2932 (1982).
[9] R. K. Williams, W. H. Butler, R. S. Graves, and J. P. Moore, Phys. Rev. B **28**, 6316 (1983).
[10] P. G. Klemens and R. K. Williams, Int. Met. Rev. **31**, 197 (1986).
[11] R. Venkatasubramanian, E. Siivola, T. Colpitts, and B. O'Quinn, Nature **413**, 597 (2001).
[12] Z. Lin, L. V. Zhigilei, and V. Celli, Phys. Rev. B **77**, 075133 (2008).
[13] J. A. Bain, J. A. Malen, M. Jeong, and T. Ganapathy, MRS Bull. **43**, 112 (2018).
[14] M. M. Maqableh, X. Huang, S.-Y. Sung, K. S. M. Reddy, G. Norby, R. H. Victora, and B. J. H. Stadler, Nano Lett. **12**, 4102 (2012).
[15] D. Josell, S. H. Brongersma, and Z. Tőkei, Annu. Rev. Mater. Res. **39**, 231 (2009).
[16] W. G. Ma, H. D. Wang, X. Zhang, and W. Wang, J. Appl. Phys. **108**, 064308 (2010).
[17] W. Ma and X. Zhang, Int. J. Heat Mass Transfer **58**, 639 (2013).
[18] G. V. Chester and A. Thellung, Proc. Phys. Soc. **77**, 1005 (1961).
[19] D. Cahen, J. R. Hahn, and J. R. Anderson, Rev. Sci. Instrum. **44**, 1567 (1973).
[20] E. Grüneisen and H. Reddemann, Ann. Phys. **412**, 843 (1934).
[21] W. K. G. Kemp, P. G. Klemens, A. K. Sreedhar, and G. K. White, Lond. Edinb. Dublin Philos. Mag. J. Sci. **46**, 811 (1955).
[22] *Thermal Conductivity: Theory, Properties, and Applications*, edited by T. M. Tritt (Kluwer Academic/Plenum Publishers, New York, 2004).
[23] P. M. Rowell, Proc. R. Soc. London, Ser. A **254**, 542 (1960).
[24] M. Yao, M. Zebarjadi, and C. P. Opeil, J. Appl. Phys. **122**, 135111 (2017).
[25] G. Leibfried, in *Handbuch Der Physik*, edited by S. Flügge (Springer-Verlag, Berlin, 1955), pp. 104–324.
[26] G. A. Slack, in *Solid State Physics*, edited by H. Ehrenreich, F. Seitz, and D. Turnbull (Academic Press, New York, 1979), pp. 1–71.
[27] N. Stojanovic, D. H. S. Maithripala, J. M. Berg, and M. Holtz, Phys. Rev. B **82**, 075418 (2010).
[28] P. Debye, Ann. Phys. **344**, 789 (1912).
[29] A. H. Wilson, Math. Proc. Cambridge Philos. Soc. **33**, 371 (1937).
[30] P. Heino and E. Ristolainen, Microelectron. J. **34**, 773 (2003).
[31] S. Poncé, E. R. Margine, C. Verdi, and F. Giustino, Comput. Phys. Commun. **209**, 116 (2016).
[32] S. Poncé, E. R. Margine, and F. Giustino, Phys. Rev. B **97**, 121201 (2018).
[33] F. Giustino, Rev. Mod. Phys. **89**, 015003 (2017).
[34] S. Li, Z. Tong, and H. Bao, J. Appl. Phys. **126**, 025111 (2019).
[35] C. Li, N. K. Ravichandran, L. Lindsay, and D. Broido, Phys. Rev. Lett. **121**, 175901 (2018).
[36] A. Jain and A. J. H. McGaughey, Phys. Rev. B **93**, 081206 (2016).
[37] Y. Wang, Z. Lu, and X. Ruan, J. Appl. Phys. **119**, 225109 (2016).
[38] Z. Tong and H. Bao, Int. J. Heat Mass Transfer **117**, 972 (2018).
[39] Y. Chen, J. Ma, and W. Li, Phys. Rev. B **99**, 020305 (2019).
[40] G. P. Srivastava, *The Physics of Phonons* (CRC Press, Boca Raton, FL, 1990).
[41] J. M. Ziman, *Electrons and Phonons: The Theory of Transport Phenomena in Solids* (Oxford University Press, Oxford, UK, 2001).
[42] A. K. Vallabhaneni, D. Singh, H. Bao, J. Murthy, and X. Ruan, Phys. Rev. B **93**, 125432 (2016).
[43] G. D. Mahan, *Many-Particle Physics*, 3rd ed. (Kluwer Academic/Plenum Publishers, New York, 2000).
[44] H. Xie, J. Yan, X. Gu, and H. Bao, J. Appl. Phys. **125**, 205104 (2019).
[45] C. L. Julian, Phys. Rev. **137**, A128 (1965).
[46] P. Giannozzi, S. Baroni, N. Bonini, M. Calandra, R. Car, C. Cavazzoni, D. Ceresoli, G. L. Chiarotti, M. Cococcioni, I. Dabo, A. Dal Corso, S. de Gironcoli, S. Fabris, G. Fratesi, R. Gebauer, U. Gerstmann, C. Gougoussis, A. Kokalj, M. Lazzeri, and L. Martin-Samos *et al.*, J. Phys. Condens. Matter **21**, 395502 (2009).
[47] W. Li, J. Carrete, N. A. Katcho, and N. Mingo, Comput. Phys. Commun. **185**, 1747 (2014).
[48] See Supplemental Material at http://link.aps.org/supplemental/10.1103/PhysRevB.100.144306 for details on the simulations, optimized lattice constants, **q** and **k** meshes in electron-phonon interpolation, convergence tests, spin-orbital coupling effect, Grüneisen parameter and Debye temperature, phonon dispersion, phonon density of states, phonon-phonon scattering rate, phonon-electron scattering rate, electron band structure, electron density of states, electron-phonon scattering rate, Eliashberg spectral function, and definition of accumulation function.
[49] J. Noffsinger, F. Giustino, B. D. Malone, C.-H. Park, S. G. Louie, and M. L. Cohen, Comput. Phys. Commun. **181**, 2140 (2010).
[50] N. Marzari, A. A. Mostofi, J. R. Yates, I. Souza, and D. Vanderbilt, Rev. Mod. Phys. **84**, 1419 (2012).
[51] N. Troullier and J. L. Martins, Phys. Rev. B **43**, 1993 (1991).
[52] J. P. Perdew and Y. Wang, Phys. Rev. B **45**, 13244 (1992).

[53] J. P. Perdew, K. Burke, and M. Ernzerhof, Phys. Rev. Lett. **77**, 3865 (1996).
[54] W. Li, Phys. Rev. B **92**, 075405 (2015).
[55] J. Ma, A. S. Nissimagoudar, and W. Li, Phys. Rev. B **97**, 045201 (2018).
[56] R. W. Powell and Y. S. Toulou, Science **181**, 999 (1973).
[57] Y. S. Touloukian, *Thermophysical Properties of Matter: Thermal Conductivity of Metallic Elements and Alloys* (IFI/Plenum Data Corporation, New York, 1970).
[58] C. Y. Ho, R. W. Powell, and P. E. Liley, *Thermal Conductivity of the Elements: A Comprehensive Review* (National Standard Reference Data, 1974).
[59] P. G. Klemens, in *Thermal Conductivity of Pure Metals and Alloys*, Landolt-Börnstein - Group III Condensed Matter 15c: Condensed Matter, edited by O. Madelung and G. K. White (Springer-Verlag, Berlin, Heidelberg, 1991), pp. 460–496.
[60] Y. Terada, K. Ohkubo, T. Mohri, and T. Suzuki, Mater. Trans. **43**, 3167 (2002).
[61] C. Kittel, *Introduction to Solid State Physics*, 8th ed. (Wiley, Hoboken, NJ, 2005).
[62] G. A. Slack, J. Phys. Chem. Solids **34**, 321 (1973).
[63] P. Nath, J. J. Plata, D. Usanmaz, C. Toher, M. Fornari, M. Buongiorno Nardelli, and S. Curtarolo, Scr. Mater. **129**, 88 (2017).
[64] S. Y. Savrasov and D. Y. Savrasov, Phys. Rev. B **54**, 16487 (1996).
[65] D. A. Papaconstantopoulos, L. L. Boyer, B. M. Klein, A. R. Williams, V. L. Morruzzi, and J. F. Janak, Phys. Rev. B **15**, 4221 (1977).
[66] R. Bauer, A. Schmid, P. Pavone, and D. Strauch, Phys. Rev. B **57**, 11276 (1998).
[67] D. Gall, J. Appl. Phys. **119**, 085101 (2016).